Magnetic Manipulation of Nanorods in the Nucleus of Living Cells

Alfredo Celedon,[†‡*] Christopher M. Hale,[‡§] and Denis Wirtz[‡§*]
[†]Department of Mechanical Engineering, Pontificia Universidad Católica de Chile, Santiago, Chile; and [‡]Physical Sciences in Oncology Center and [§]Department of Chemical and Biomolecular Engineering, The Johns Hopkins University, Baltimore, Maryland

ABSTRACT The organization of chromatin in the cell nucleus is crucial for gene expression regulation. However, physically probing the nuclear interior is challenging because high forces have to be applied using minimally invasive techniques. Here, magnetic nanorods embedded in the nucleus of living cells are subjected to controlled rotational forces, producing micron-sized displacements in the nuclear interior. The resulting time-dependent rotation of the nanorods is analyzed in terms of viscoelastic parameters of the nucleus, in wild-type and Lamin A/C deficient cells. This method and analysis reveal that Lamin A/C knockout, together perhaps with other changes that result from the knockout, induce significant decreases in the nuclear viscosity and elasticity.

INTRODUCTION

The precise organization of interphase chromatin in the nucleus of eukaryotes cells is crucial for the regulation of gene expression. A nuclear scaffold is thought to define the spatial organization of interphase chromatin (1). Even if important elements of the nuclear architecture have been identified, such as the nuclear lamina, the organization of interphase chromatin is poorly understood. The associated physical properties of the nucleus interior, such as nuclear viscoelasticity that controls the dynamics of the transcription machinery, are also largely unknown (2). The nuclear lamina is mainly constituted of polymers of Lamin A/C and Lamin B, which form a dense network that coats the surface of the inner nuclear envelope leaflet and also interdigitates the nucleoplasm (3). Several nuclear proteins interact with lamins, including core histones (4), BAF (5) and HP1 (6), and linkers of nucleoskeleton to cytoskeleton complexes (7,8), which mediate physical connections between chromatin, the nuclear lamina, and the cytoskeleton, which in turn participate in gene regulation. Studies in *Drosophila melanogaster* indicate that lamins bind to transcriptionally inactive chromatin (9) and chromatin anchorages to the nuclear lamina are critically involved in delimiting regions with different gene activation levels (10).

To study the physical properties of the nuclear interior, it is crucial to have tools able to precisely apply forces and deform the nuclear interior. The structure of the first level of nuclear organization, the chromatin fiber, has been studied using single-molecule experiments. Single reconstituted fibers have been pulled (11–13) and twisted (14,15) in order to obtain their physical properties. At a higher level of organization, the structure of isolated metaphase chromosomes has been studied in pulling experiments using micropipettes (16,17). However, the structure of interphase chromatin needs to be studied in situ in the cell nucleus, which greatly complicates the experimental requirements. Particle microrheology (18) and magnetic tweezers (19) have been used to assess the nuclear interior by the spontaneous or forced lateral movements of spherical probes.

In the magnetic-tweezers technique, magnetic particles are manipulated with a magnetic field, with the advantage of allowing researchers both to study a small nuclear volume noninvasively and to apply forces in the nuclear interior. However, the method faces a major challenge. Because small particles are required (<1 μm) and applied forces decrease proportionally with particle volume, magnetic forces are not sufficiently strong to deform the nuclear interior. A recently developed technique partially circumvents this problem by using microfabricated poles to create a high magnetic field gradient (20). Using this technique, Vries et al. (19) displaced a 1-μm bead over distances of $<$200 nm in the nuclear interior. However, the technique is complicated because the cell needs to be positioned at <10 μm from the tips of the microfabricated poles. Furthermore, a constant magnetic field gradient between the poles is difficult to ensure and therefore the exact force applied on the bead is uncertain.

Here, we demonstrate what to our knowledge is a new method to apply large rotational forces within the nuclear interior without the need of microfabricated poles (Fig. 1). To our knowledge, this method is the first noninvasive technique able to produce micron-sized displacements inside the nucleus. The magnetic field strength B is constant in at least a ~5×5 mm^2 region on the cell culture dish and therefore the torque applied does not depend on the position of the probe within the cell. The strength B can be readily increased by bringing the magnets closer to the sample, producing torques at least 10 times larger than the ones shown in this work (Fig. 2). Because the magnets are located far from the cells, the technique has the potential to be applied to cells in a tissue.

We use this technique to measure the viscoelastic properties of nuclei of wild-type ($LMNA^{+/+}$) and Lamin A/C-deficient ($LMNA^{-/-}$) mouse embryonic fibroblasts

Submitted May 11, 2011, and accepted for publication September 8, 2011.

*Correspondence: alfredo.celedon@gmail.com or wirtz@jhu.edu

Editor: Petra Schwille.

0006-3495/11/10/1880/7 $2.00

doi: 10.1016/j.bpj.2011.09.008

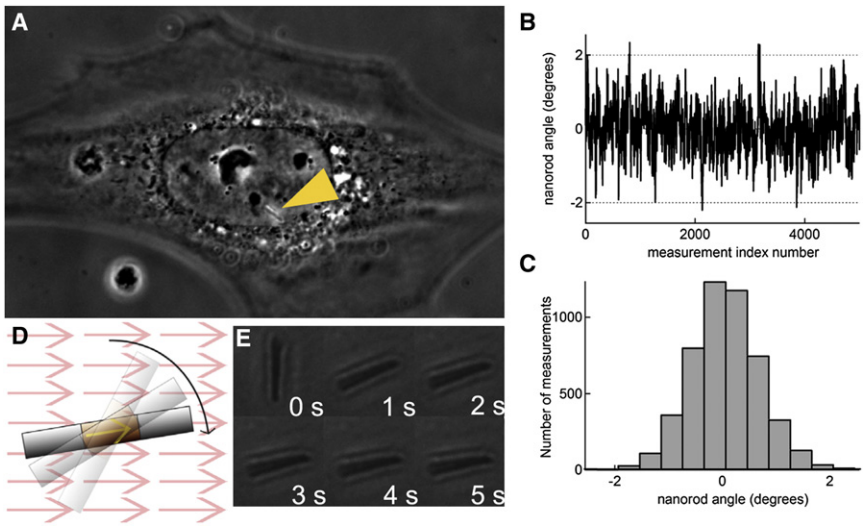

FIGURE 1 Controlled angular movements of magnetic nanorods to measure the rotational microrheology of the interphase nucleus. (*A*) Phase contrast micrograph of a wild-type mouse embryonic fibroblast (WT $LMNA^{+/+}$ MEF) with a nanorod lodged in its nucleus (*arrow*). Magnetic nanorods were transferred to the nucleus of live cells using ballistic injection. (*B*) Brownian angular fluctuations of a nanorod under the magnetic field employed in the experiments. (*C*) The corresponding angular distribution of the nanorod. This data allowed us to obtain the angular trap stiffness (see text). (*D*) Pt/Ni/Pt nanorod rotates as a result of a sudden 90° change in the direction of the magnetic field. Analysis of the time-dependent rotation of the nanorod is used to evaluate the angular viscoelastic properties of the interphase nucleus. (*E*) Typical time sequence of nanorod rotation inside the nucleus, imaged with bright-field microscopy; a fast phase of rotation is followed by a slow phase of rotation toward 90°.

(MEFs). Our measurements suggest that Lamin A/C participates in the organization of the nuclear material regulating the mechanical properties of the nuclear interior. The dramatic difference observed in $LMNA^{-/-}$ MEFs can be explained by a loss of Lamin A/C-mediated chromatin anchor points and/or a loss of lamin networks interdigitating the nucleoplasm volume.

MATERIALS AND METHODS

Cell culture

Wild-type mouse embryonic fibroblasts ($LMNA^{+/+}$ MEFs) and MEFs obtained from Lamin A/C knockout mouse ($LMNA^{-/-}$ MEFs) were cultured in Dulbecco's modified Eagle's medium (Sigma, St. Louis, MO) complemented with 10% bovine calf serum (BCS; American Type Culture Collection, Manassas, VA), 100 units/ml penicillin, and 100 μg/ml streptomycin (Sigma) and maintained at 37°C, 5% CO_2 and humidified atmosphere. Cells were passaged every 3–4 days and discarded after 15 passages. Previous work by our group and others has identified phenotypic differences between WT and $LMNA^{-/-}$ cells, including cell migration and polarization (21).

Nanorod fabrication

Platinum/Nickel/Platinum (Pt/Ni/Pt) nanorods were fabricated by electrochemical deposition in the pores of an aluminum oxide membrane (Whatman, Springfield Mill, England), as previously described (15). Briefly, segments of different metals were added to the nanorods by sequentially changing the metallic ions of the electrolytic solution. Each segment length was controlled by the total electric charge that circulated in the electrochemical cell during the deposition. A sacrificial segment of Cu was deposited first from a Cu sulfate solution. Pt was deposited from a hexachloroplatinate solution and Ni from a Ni sulfate solution. The length of the Ni segment determines the strength of the magnetic dipole of the nanorod. The nonmagnetic Pt segments increase the length of the nanorod without significantly affecting its magnetic properties.

After deposition, nanorods were released by etching the Copper in a BTP copper etchant bath (Transene, Danvers, MA) for 8 h at 40°C and the membrane in 2 M KOH at 65°C overnight. The nanorods were finally sonicated and suspended in ethanol for storage. The nanorods have a distribution of diameters and lengths, with an approximate average of 200 nm in diameter and 1.5 μm in length. We used scanning electron microscopy to measure the pore diameter where the nanorods were deposited while the length of the nanorods was measured using bright-field microscopy. The measured nanorod length is 1.46 $\pm$ 0.05 μm ($\pm$ SD). Because the pores are not perfectly circular, an apparent diameter was obtained using

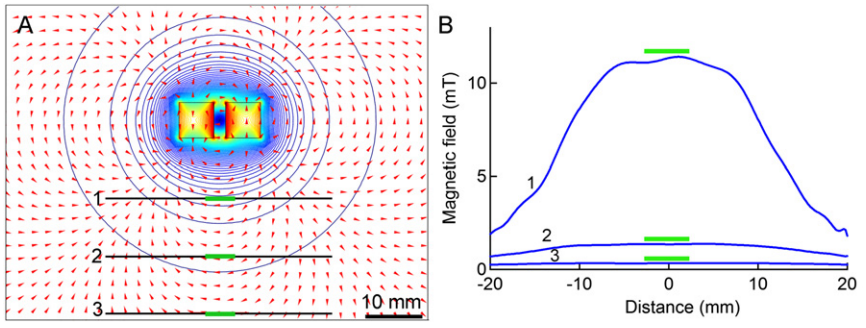

FIGURE 2 Simulation of the magnetic field *B* using finite elements. (*A*) Two-dimensional slice from a three-dimensional numerical simulation performed using COMSOL (v.3.5; http://www.comsol.com/). (*Contour lines*) The norm of magnetic field *B*. (*Arrows*) The direction of magnetic field *B*. The magnetic field is horizontal in the regions directly below the pair of magnets (*thick horizontal segments*) (*B*) The norm of magnetic field *B* along the black paths 1, 2, and 3 shown in panel *A* at 10, 20, and 30 mm from the magnets, respectively. The magnetic field norm is constant in the central 5 mm (*thick horizontal segments*), showing that the calibration obtained at one point allows precise calculation of torques in a large region. The experiments in this work were done with the pair of magnets at 20 mm from the sample (path 2). The magnetic field is almost 10 times larger on path 1 than on path 2, showing the potential of our technique to apply significantly larger torques than the ones shown here.

the formula $D = 2$*sq rt(area/π). The average pore diameter is 208 $\pm$ 26 nm ($\pm$ SD).

Introduction of nanorods into the cells

The nanorods were separated from the ethanol in which they were stored by approaching a magnet to the tube wall. The nanorods cluster against the vessel wall in less than a minute and the supernatant is removed using a micropipette. The rods were first suspended in Standard Buffer (10 mM phosphate buffer, pH = 8, 0.1% Tween-20) complemented with 1 mg/ml bovine serum albumin, incubated for 20 min and resuspended in Standard Buffer and sonicated for 1 min. Nanorods were ballistically injected in the cytoplasm or nucleus of cells using a Biolistic PDS-1000/HE particle delivery system (BioRad, Richmond, CA). Nanorods were ballistically injected in cells at 80% confluence. Macrocarriers were coated with nanorods (~10^5 nanorods) and 1100-psi rupture disks were used. After bombarding with nanorods, cells were washed three times to prevent cellular endocytosis of the nanorods. Cells were given at least 8 h to recover postbombardment. Cells were then replated to remove nanorods that were outside of the cells, typically on the substrate surface. Replated cells were allowed to spread for 24 h before experiments. The nanorods were found preferentially close to the nucleus membrane (within ≈ 5 μm from the membrane).

Driven rotation and high-resolution tracking of nanorods

Experiments were conducted using an inverted microscope (Eclipse TE2000-E; Nikon, Melville, NY) equipped with a linear stage (460P-XYZ; Newport, Irvine, CA) that holds a custom-made rotational stage with a couple of parallel Neodymium-Iron-Boron permanent magnets (K&J Magnetics, Jamison, PA) placed 2 mm from each other. Each magnet is 6 mm in size and of grade N42. The sample is illuminated through the space between the magnets. The distance between the magnets and the cells is 20 mm for all the experiments. Magnets in this configuration produced a magnetic field parallel to the glass substrate, which orient any nanorods that are parallel to the glass substrate. Samples are observed using a high magnification 60× oil-immersion objective lens. Time-lapsed images were collected with a charge-coupled device digital camera (ORCA-ER; Hamamatsu, Hamamatsu City, Japan) at a frame rate of at least 10 Hz. The videos were analyzed on a PC using customized software written in MATLAB (version 7.1.0.246; The MathWorks, Natick, MA). The time-dependent angle and position of the nanorod at each frame were obtained by fitting an ellipse to the largest dark area in the image (Fig. 1 *E*).

Experiments consisted of a rotation of the magnetic field parallel to the glass substrate while measuring the response of the nanorod for 180 s. Because the magnetic field is always parallel to the substrate, it induces a rotation of the nanorod parallel to the substrate. A rotation perpendicular to the substrate would reduce the apparent length of the nanorod. We do not see changes on nanorod length during rotation. We tested reversibility by rotating the magnetic back to its initial orientation. We also tested the effect of three sequential rotations in the same direction. No significant difference in the nanorod response was observed either in reverse rotations or in sequential rotations.

The strength with which the magnetic field orients the nanorod dipole was measured by tethering a nanorod to the glass substrate using a10-kbp DNA molecule. This experiment was conducted in water. The nanorod was pulled using the magnets in the same configuration used for the cell experiments. While leaving the orientation of the magnets constant, we recorded the angular fluctuation of the nanorod. The torque applied by the magnetic field to the nanorod is $\boldsymbol{\tau} = \boldsymbol{m} \times \boldsymbol{B} \sim mB\theta$, where m is the nanorod magnetic dipole and B is the applied magnetic field. The product mB was obtained from the histogram of 5000 measurements of the angle of the nanorod. We applied the equipartition theorem to find $mB = k_BT/\langle\delta\theta^2\rangle$. We conducted this experiment for three different nanorods and found $mB = 8410 \pm 690\ k_BT$. This value is a direct measurement of the strength of the magnetic field that orients the nanorods in the cells. The presence of the DNA molecule does not interfere with the measurements because the twist stiffness of the 10-kbp molecule is ~$2.2 \times 10^{-2}\ k_BT$, which is much lower than the product mB.

RESULTS AND DISCUSSION

Rotational forces or torques were applied to magnetic nanorods located inside the nucleus in order to deform the nuclear interior (Fig. 1 *A*). The magnetic torque experienced by a magnetic particle does not depend on the magnetic field gradient, as is the case of the magnetic linear force; instead, it depends on the magnetic field strength (Fig. 1 *B*), according to the formula $\boldsymbol{\tau} = \boldsymbol{m} \times \boldsymbol{B}$, where $\boldsymbol{m}$ is the dipole of the particle. We used Pt/Ni/Pt nanorods that are 200-nm diameter and 1.5 μm in length with the ferromagnetic Nickel section of 500 nm in length. This construct produced a magnetic dipole oriented in the direction of the nanorod axis. A pair of cubic permanent magnets positioned 20 mm above the cell culture dish was used to generate a horizontal magnetic field (Fig. 2). A sudden rotation of the pair of magnets by 90° rotated the magnetic field, producing a torque that tended to orient the nanorod embedded in the cellular nucleus or the cytoplasm in the new preset direction of the field. During this process, the nanorod experienced a torque equal to $mB\sin[\pi/2-\theta\ (t)]$, where $\theta(t)$ is the time-dependent angle of the nanorod with respect to the initial orientation of the field.

To calibrate the torque applied by the magnetic tweezers before experiments, we measured the strength of the angular trap, mB, using a single-molecule approach. A magnetic nanorod was tethered by a single DNA molecule to a glass slide and pulled away from the surface using the same pair of magnets and in the same relative position as in the cell experiments (see Materials and Methods). The angular fluctuations of the nanorod displayed a Gaussian distribution centered at the direction the magnetic field, $\theta = 0$ (Fig. 1, *B* and *C*). The equipartition theorem allowed us to obtain $mB = 8410 \pm 690\ k_BT$ (see Materials and Methods). Fig. 2 *B* shows that the simulated magnetic field at 20 mm from the magnets (path 2) is 1.4 mT, therefore using the estimated dipole of a 500-nm Nickel segment ($1.8 \cdot 10^{-14}$ A·m^2), with the prediction of the angular trap strength being 6270 k_BT, close to the experimental value. The strength of the angular trap can be easily changed in our setting by moving the magnets vertically, closer to or farther from the glass slide. We used the same angular trap strength in all the experiments described in this work.

This magnetic trap applied a rotational force sufficient to rotate the nanorod inside the nucleus producing a large deformation of the nuclear interior. Fig. 1 *E* shows a typical time sequence of the rotational movement of a nanorod embedded in the nucleus. The magnetic field and the nanorod had the same orientation before $t = 0$ (pointing

upwards). At $t = 0$, the magnetic field was rotated by 90°. The nanorod angle θ changed rapidly in the first second and slowly during the following seconds.

The evolution of θ after a change of the magnetic field depended on the properties of the nuclear interior (Fig. 3). We used a custom-made code to track $\theta(t)$ from bright-field images of nanorods taken at 10 frames/s in the nucleus and in the cytoplasm of $LMNA^{+/+}$ and $LMNA^{-/-}$ MEFs. Fig. 3 *C* shows representative evolutions of $\theta(t)$ in these experiments. Curves obtained in $LMNA^{+/+}$ nuclei (*green symbols*) showed that the nanorods did not reach the angle of the magnetic field (90°) within seconds; instead, they suffered a fast initial rotation and reached an angle of ~40° and then slowly crept toward the direction of the field. We defined the residual angle as the difference between the magnetic field angle and the angle of the nanorod at 10 s. The existence of a residual angle suggests that the nuclear material has a significant elastic component, exerting forces that grow with the applied deformation. This observation agrees with measurements that found a high nuclear elasticity (18,19,22,23).

The response of nanorods in the interphase nucleus of $LMNA^{-/-}$ MEFs presented a significantly smaller residual angle than the one obtained for nanorods in the interphase nucleus of $LMNA^{+/+}$ MEFs (*red symbols* in Fig. 3). This striking difference suggests that Lamin A/C proteins are involved in maintaining the nuclear internal structure, by keeping the position of chromatin and/or through internal networks of lamin proteins. We show for comparison the response of nanorods in the cytoplasm (*blue symbols*). The initial phase of rotational movement was significantly faster than for nanorods lodged in the nucleus, and the curves presented little or no residual angle. We found no significant difference between nanorods' responses in the cytoplasm of $LMNA^{+/+}$ MEFs and those in the cytoplasm of $LMNA^{-/-}$ MEFs. This result was expected because the strength of the magnetic field was optimized to produce curves that reveal the nucleus viscoelastic properties. Therefore, the magnetic field was too strong to interrogate the cytoplasm. Nanorods in the cytoplasm reached the direction of the magnetic field within ~1 s, producing curves that do not contain enough information to detect the relatively small viscoelastic differences.

To obtain a precise measurement of the rheological properties of the nucleus, we first searched for a viscoelastic model able to represent the evolution of $\theta(t)$ after a sudden change in magnetic field orientation. Different assemblies of torsional dashpots and torsional springs were considered and used to approximate the properties of the nuclear interior (Fig. 3 *A*). Each assembly generated a different time-dependent profile for the angle in response to external torques (see the Supporting Material).

Fig. 3 *B* shows theoretical curves fit to the experimental data using models I–IV. These models correspond to torsional dashpot and spring in series (Model I) and parallel (Model II), a torsional spring in series with a second element composed of a torsional spring in parallel with a torsional dashpot (Model III), and a torsional dashpot in series with a second element composed of a torsional spring in parallel with a torsional dashpot. Models I–III generated responses that were significantly different from the experimental data. Model I could not hold a residual angle and models II and III reached their final angle after a fast rotation. Only model IV had a fast initial rotation and did not reach its final angle as a result of it. After the fast initial rotation, model IV rotated slowly toward 90°. We fitted the angular data from each experiment with model IV (*solid curves* in Fig. 3 *C*) using an unconstrained nonlinear optimization function to minimize the sum of the squared errors. As a result, we obtained the three fitting parameters: the dashpots' damping coefficients (γ_1, γ_2) and the spring constant (k_1), which are related to the viscosities (η_1, η_2) and the shear modulus (μ) of the material (see the Supporting Material).

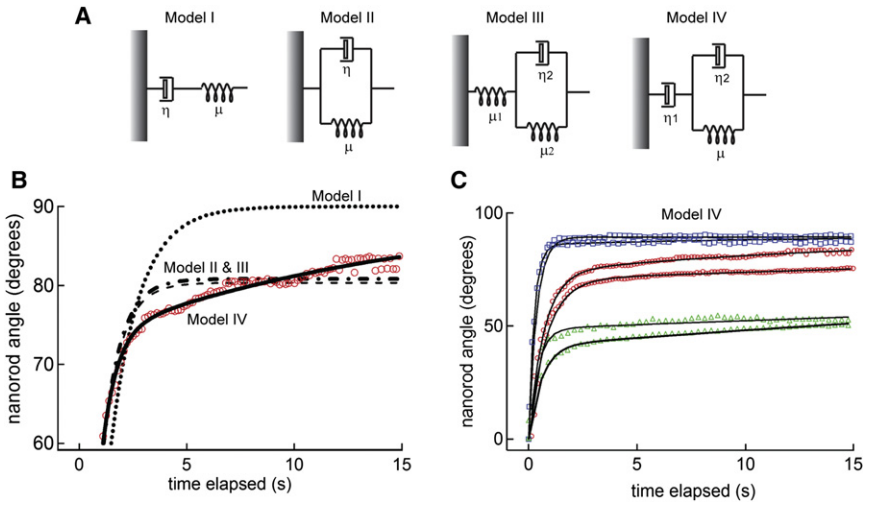

FIGURE 3 Rotation of nanorods embedded in the nucleus after a change in magnetic field direction. (*A*) Simple viscoelastic spring-dashpot models used to fit nanorod angular responses after a rapid change in magnetic field direction. These models include elastic spring and viscous dashpot in series (model I), spring and dashpot in parallel (model II), spring in series with a spring and dashpot in parallel (model III), and a dashpot in series with a spring and dashpot in parallel (model IV). Additional details about the fits are in the Supporting Material. (*B*) Only model IV led to a good fit of the time-dependent rotation of nanorods in the nucleus of a WT cells. (*C*) Time-dependent rotations and associated fits using model IV for nanorods embedded in the nucleus of an $LMNA^{+/+}$ cell (*green triangles*) and an $LMNA^{-/-}$ cell (*red circles*), and nanorods in their respective cytoplasm (*blue squares*). The rotational responses are fit with model IV.

Fig. 4 summarizes our measurements of viscoelastic properties obtained using the method described above. The nucleus of $LMNA^{+/+}$ MEFs is characterized by the rheological parameters $\eta_1 = 25.1 \pm 4.1$ Pa·s, $\eta_2 = 0.57 \pm 0.07$ Pa·s, and $\mu = 0.48 \pm 0.07$ Pa. For nuclei of $LMNA^{-/-}$ cells, we obtained $\eta_1 = 3.7 \pm 0.7$ Pa·s, $\eta_2 = 0.51 \pm 0.03$ Pa·s, and $\mu = 0.15 \pm 0.01$ Pa. Finally, for the cytoplasm, $\eta_1 = 1.19 \pm 0.04$ Pa·s, $\eta_2 = 0.70 \pm 0.1$ Pa·s, and $\mu = 0.10 \pm 0.02$ Pa.

The finding that model IV is able to explain the differential response of nanorods in WT and $LMNA^{-/-}$ cells suggests that three parameters are sufficient to describe a wide range of nuclear conditions. This is practically convenient because it defines a simple way of charactering and comparing different nuclei. Model IV represents a material that has two characteristics regimes depending on the deformation rate and the total deformation. The other models have only one characteristic behavior. In the nanorod evolution curves, the two regimes can be seen in the fast initial rotation and the much slower one that follows. Mathematically, model IV predicts an evolution with a function consisting of two exponentials (see the Supporting Material). At high deformation rate and low total deformation, the independent dashpot (*dashpot* with constant η_1 in Fig. 4) basically does not deform because of the higher resistance it opposes in comparison to the combination of dashpot and spring in parallel (*dashpot* with constant η_2 and *spring* with constant μ in Fig. 3).

Note that η_1 is an order-of-magnitude higher than η_2 for nanorods inside the nucleus. In this regime, the material has a solidlike behavior because of the relative importance of the spring elastic response. Instead, at low deformation rate and high total deformation, the independent dashpot deforms significantly because it opposes a lower resistance than the combination of dashpot and spring in parallel. In this regime, the material has a liquidlike behavior because of the relative importance of the dashpot viscous response. From a molecular point of view, the elastic, solidlike regime probably originates from fibers that bend and stretch without significant rearrangement. The viscous, liquidlike regime, instead, probably originates from fibers rearranging and sliding with respect to each other and the friction that this process involves.

Our measurements indicate that the viscosity and shear modulus of the cell nucleus are significantly affected in the absence of Lamin A/C. $LMNA^{-/-}$ cells had a viscosity seven times lower than $LMNA^{+/+}$ and a shear modulus three times lower. Previous measurements of Lamin A/C-deficient cells found decreased cellular (24) and nuclear stiffness (25). However, it was not clear whether the change in mechanical properties was the result of alteration of the nuclear lamina only or if alterations of the nuclear interior were also present. Our result shows that the mechanical properties of the nuclear interior are changed in $LMNA^{-/-}$ cells. This result suggests that Lamin A/C mediates anchor points with chromatin and/or it forms

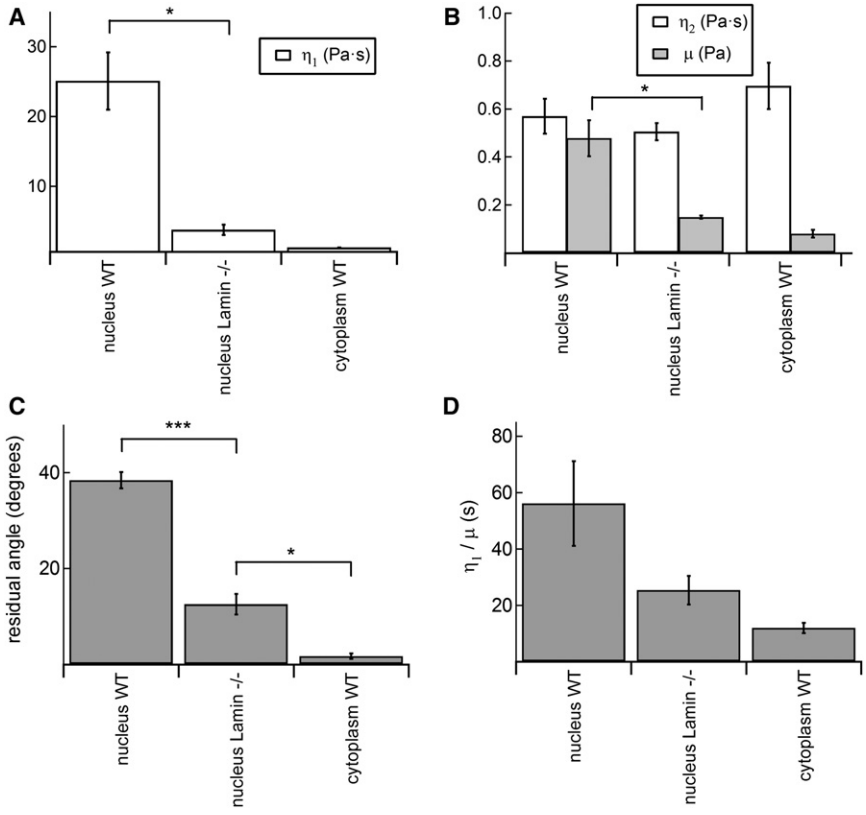

FIGURE 4 Lamin A/C deficiency causes defects in rotational viscoelasticity of the nucleus. (*A*) The viscosity η_1 of $LMNA^{+/+}$ nuclei is seven times higher than the viscosity of $LMNA^{-/-}$ nuclei and 21 times higher than the viscosity of the cytoplasm. (*B*) The shear modulus, μ, of $LMNA^{+/+}$ nuclei is three times higher than the shear modulus of $LMNA^{-/-}$ nuclei. The viscosity η_2 are not significantly different. (*Asterisk*) $P < 0.05$ (Student *t*-test; $N = 7$). (*C*) Angle difference between the direction of the magnetic field and the nanorod 10 s after magnetic field rotation (*residual angle*). (*D*) Relaxation time, $t_1 = \mu/\eta_1$, describing the time it takes nanorods subjected to an applied magnetic field to reach a steady state for nuclei in $LMNA^{-/-}$ and $LMNA^{+/+}$ cells, and the cytoplasm of a $LMNA^{+/+}$ cell.

internal networks that determine the organization of the nucleus interior.

The shear modulus of WT cells obtained in our experiments correspond to a Young's modulus of the nucleus $Y = 3\mu = 1.5$ Pa. Previous measurements of WT HeLa cells using a 1-μm-diameter magnetic particle obtained an elasticity of 250 Pa (19). The apparent disagreement is probably a result of the different dimensions of the probes. The diameter of the nanorods used in our experiments is 200 nm. Indeed, particle tracking measurements using 100-nm diameter nanospheres (18) found a Young's modulus of 18 Pa for Swiss 3T3 fibroblast nucleus, closer to our measurements. If these differences are the result of probe size, then important structural elements of the nuclear interior are spaced ~1 μm and are not sensed with smaller probes. Differences in nuclear internal elasticity could arise also from different chromatin organization in the different cell lines used in the experiments.

Nanorod introduction into the nucleus probably alters the local structure of chromatin and other internal structure of the nucleus. However, our results indicate that this alteration is not significant because it does not impair cell functions, such as cell shape and motility. Because measurements were obtained >32 h after introduction of the nanorods, our measurements captured the internal properties of viable cells. The difference observed between wild-type and *LMNA* knockouts shows that the technique produces relevant information of the nucleus interior.

CONCLUSION

We have described what to our knowledge is a new method to manipulate particles in the interior of the cell nucleus. A calibrated magnetic torque produces rotation of a nanorod inside the nucleus of a living cell. The analysis of the rod motion generates precise information of the rheological properties of the medium where the nanorod is located. These rheological properties are the result of the nucleus internal architecture and interphase chromatin organization. We found that the nucleus of Lamin A/C-deficient cells have lower elasticity than that of WT cells, which suggests that anchor points mediated by Lamin A/C and/or internal networks of Lamin A/C are critical to nuclear spatial organization. However, our experiments did not exclude potential secondary effects derived from the lack of Lamin A/C. Future experiments can systematically map the viscoelastic properties of the nucleus to help elucidate the global structure of the nuclear interior. Furthermore, the capacity to produce controlled large displacements inside the nucleus can be used together with imaging techniques (26) to assess the effects in gene expression of nuclear structural changes. Magnetic nanorods apply large magnetic forces using magnets located far from the cells (several centimeters). Therefore, using this technique, several nuclei in a tissue or an organ can be deformed at the same time.

SUPPORTING MATERIAL

Additional information with supporting equations is available at http://www.biophysj.org/biophysj/supplemental/S0006-3495(11)01062-9.

A.C. gratefully acknowledges support from the Chilean Fondo Nacional de Desarrollo Científico y Tecnológico, 11100416. A.C. and D.W. gratefully acknowledge support from National Institutes of Health grant R03TW008718 from the Fogarty International Center. D.W. gratefully acknowledges support from National Institutes of Health R01GM084204 and U54CA143868.

REFERENCES

1. Misteli, T. 2005. Concepts in nuclear architecture. *Bioessays.* 27: 477–487.
2. Thomas, M. C., and C. M. Chiang. 2006. The general transcription machinery and general cofactors. *Crit. Rev. Biochem. Mol. Biol.* 41:105–178.
3. Goldman, R. D., Y. Gruenbaum, …, T. P. Spann. 2002. Nuclear lamins: building blocks of nuclear architecture. *Genes Dev.* 16:533–547.
4. Taniura, H., C. Glass, and L. Gerace. 1995. A chromatin binding site in the tail domain of nuclear lamins that interacts with core histones. *J. Cell Biol.* 131:33–44.
5. Laguri, C., B. Gilquin, …, S. Zinn-Justin. 2001. Structural characterization of the LEM motif common to three human inner nuclear membrane proteins. *Structure.* 9:503–511.
6. Polioudaki, H., N. Kourmouli, …, S. D. Georgatos. 2001. Histones H3/H4 form a tight complex with the inner nuclear membrane protein LBR and heterochromatin protein 1. *EMBO Rep.* 2:920–925.
7. Razafsky, D., and D. Hodzic. 2009. Bringing KASH under the SUN: the many faces of nucleo-cytoskeletal connections. *J. Cell Biol.* 186:461–472.
8. Khatau, S. B., C. M. Hale, …, D. Wirtz. 2009. A perinuclear actin cap regulates nuclear shape. *Proc. Natl. Acad. Sci. USA.* 106:19017–19022.
9. Pickersgill, H., B. Kalverda, …, B. van Steensel. 2006. Characterization of the *Drosophila melanogaster* genome at the nuclear lamina. *Nat. Genet.* 38:1005–1014.
10. Gerasimova, T. I., K. Byrd, and V. G. Corces. 2000. A chromatin insulator determines the nuclear localization of DNA. *Mol. Cell.* 6:1025–1035.
11. Cui, Y., and C. Bustamante. 2000. Pulling a single chromatin fiber reveals the forces that maintain its higher-order structure. *Proc. Natl. Acad. Sci. USA.* 97:127–132.
12. Bennink, M. L., S. H. Leuba, …, J. Greve. 2001. Unfolding individual nucleosomes by stretching single chromatin fibers with optical tweezers. *Nat. Struct. Biol.* 8:606–610.
13. Brower-Toland, B., D. A. Wacker, …, M. D. Wang. 2005. Specific contributions of histone tails and their acetylation to the mechanical stability of nucleosomes. *J. Mol. Biol.* 346:135–146.
14. Bancaud, A., N. Conde e Silva, …, J. L. Viovy. 2006. Structural plasticity of single chromatin fibers revealed by torsional manipulation. *Nat. Struct. Mol. Biol.* 13:444–450.
15. Celedon, A., I. M. Nodelman, …, S. X. Sun. 2009. Magnetic tweezers measurement of single molecule torque. *Nano Lett.* 9:1720–1725.
16. Poirier, M. G., and J. F. Marko. 2003. Micromechanical studies of mitotic chromosomes. *Curr. Top. Dev. Biol.* 55:75–141.
17. Marko, J. F. 2008. Micromechanical studies of mitotic chromosomes. *Chromosome Res.* 16:469–497.
18. Tseng, Y., J. S. Lee, …, D. Wirtz. 2004. Micro-organization and viscoelasticity of the interphase nucleus revealed by particle nanotracking. *J. Cell Sci.* 117:2159–2167.

19. de Vries, A. H., B. E. Krenn, …, J. S. Kanger. 2007. Direct observation of nanomechanical properties of chromatin in living cells. *Nano Lett.* 7:1424–1427.

20. de Vries, A. H., B. E. Krenn, …, J. S. Kanger. 2005. Micro magnetic tweezers for nanomanipulation inside live cells. *Biophys. J.* 88: 2137–2144.

21. Lee, J. S., C. M. Hale, …, D. Wirtz. 2007. Nuclear Lamin A/C deficiency induces defects in cell mechanics, polarization, and migration. *Biophys. J.* 93:2542–2552.

22. Mathur, A. B., G. A. Truskey, and W. M. Reichert. 2000. Atomic force and total internal reflection fluorescence microscopy for the study of force transmission in endothelial cells. *Biophys. J.* 78:1725–1735.

23. Lammerding, J., K. N. Dahl, …, R. D. Kamm. 2007. Nuclear mechanics and methods. *Methods Cell Biol.* 83:269–294.

24. Broers, J. L., E. A. Peeters, …, F. C. Ramaekers. 2004. Decreased mechanical stiffness in LMNA-/- cells is caused by defective nucleocytoskeletal integrity: implications for the development of laminopathies. *Hum. Mol. Genet.* 13:2567–2580.

25. Lammerding, J., P. C. Schulze, …, R. T. Lee. 2004. Lamin A/C deficiency causes defective nuclear mechanics and mechanotransduction. *J. Clin. Invest.* 113:370–378.

26. Vo-Dinh, T., P. Kasili, and M. Wabuyele. 2006. Nanoprobes and nanobiosensors for monitoring and imaging individual living cells. *Nanomedicine.* 2:22–30.